Cement and Concrete Composites 90 (2018) 150–160

Contents lists available at ScienceDirect

Cement and Concrete Composites

journal homepage: www.elsevier.com/locate/cemconcomp

High performance cementitious composite from alkali-activated ladle slag reinforced with polypropylene fibers

Hoang Nguyen[a], Valter Carvelli[b], Elijah Adesanya[a], Paivo Kinnunen[a,c], Mirja Illikainen[a,*]

[a] Fibre and Particle Engineering Unit, University of Oulu, Pentti Kaiteran katu 1, 90014 Oulu, Finland
[b] Department A.B.C., Politecnico di Milano, Piazza Leonardo Da Vinci 32, 20133 Milan, Italy
[c] Department of Civil and Environmental Engineering, Imperial College London, SW7 2BU London, United Kingdom

ARTICLE INFO

Keywords:
Alkali-activated slag
Polypropylene fiber
High-performance concrete
Mechanical properties
Strain hardening

ABSTRACT

Alkali-activated ladle slag (AALS) is a promising cementitious material with environmental benefits. However, the brittleness of material has been limiting the use in construction. Therefore, in this experimental investigation, different polypropylene (PP) fibers were employed as a short randomly reinforcement in cementitious matrix in order to improve mechanical performance of the AALS composites.

The study reveals that the AALS composite could gain very high ductility with an appropriate fibrous reinforcement. Fracture energy and fracture toughness of PP fiber reinforced AALS mortars increased by approximately 150 and 7.6 times, respectively, compared to the unreinforced material. Additionally, the flexural strength of the composite increased by roughly 300%. Pseudo strain hardening (PSH) behavior was observed along with multiple cracks under uniaxial tensile test. Scanning electron microscope (SEM) images confirmed the local fiber bridging effect, which resulted in the high mechanical performance of the PP-reinforced AALS.

1. Introduction

Slag from steel-making processes is an industrial by-product, that have been productized in many applications in order to avoid landfilling [1]. In 2012, approximately 21 million tons (Mt) of different slags were generated in Europe from steel-making manufacturers, and about 65% is currently utilized (e.g., cement production, road construction) [2]. Ladle slag (LS), an under-utilized slag generated in the steel-making process, accounts for roughly 1.9–2.4 Mt of yearly production in Europe. The number is an estimation considering 12–15 kg of unrecycled LS produced for every ton of crude steel and 160 Mt annual crude steel production. Currently, LS is mostly used as a filler in concrete [3,4] and there is limited research about LS used as a cementitious material. Alkali activation of slags is an interesting opportunity to manufacture cement with high recycled content and considerable environmental benefits [5,6]. The LS is barely adopted in alkali-activated materials (AAM) due to the content of free CaO which causes expansion and eventually cracks in hardening mortars. Consequently, only few investigations in literature are dealing with LS used as a precursor for AAM [7–9].

Recently, Adesanya et al. [7] developed a promising alkali-activated ladle slag (AALS) mortar by optimizing the silica and alkali contents of the material and achieved 65 MPa at 28-day compressive strength. Like other AAM mortars, this matrix exhibits brittle behavior, but has a good compressive strength. This is a good candidate to be used as concrete whose mechanical properties can be enhanced by short fibers as reinforcement.

Fiber reinforced cement and concrete in general has been investigated from 1960s in both academic studies and industrial research [10]. In past two decades, several studies have been published on using short fibers as reinforcement of cementitious materials aiming to improve the mechanical performance of mixtures. Naaman and Reinhard [11] suggested a classification for fiber reinforced concrete and the first time mentioned High Performance Fiber Reinforced Cementitious Concrete (HPFRCC). In recent years, HPFRCC was commercialized with several products such as Ductal (by Lafarge) [12], CEMTEC$_{multiscale}$ [13], and Engineered Cementitious Composites (ECC) [14].

The main purpose of using fiber in cementitious composites is to reduce the brittleness of materials by changing its post-peak behavior. The tensile behavior including post-peak strength and strain capacity of cementitious composites can be drastically improved by fibrous reinforcement [15–17]. Furthermore, the addition of micro fibers offers a favorable effect on both strain hardening and multiple cracking behavior [14,18]. These improvements lead to several practical applications for cementitious composites reported in literature including self-healing [19,20], self-consolidating [21,22], high-early-strength material [23].

* Corresponding author.
E-mail address: mirja.illikainen@oulu.fi (M. Illikainen).

https://doi.org/10.1016/j.cemconcomp.2018.03.024
Received 5 May 2017; Received in revised form 4 December 2017; Accepted 30 March 2018
Available online 31 March 2018

On the other hand, fiber reinforced cementitious composites perform well in durability tests under cyclic loading [24,25] and freeze-thaw test [26,27].

Although Portland cement-based HPFRCC has been in use for two decades, AAM-based high performance fiber reinforced composites is a new field of research. As detailed in the overview of Sakulich [28], the lack of information about high performance reinforced AAM was highlighted. Some studies have been conducted to attain a strain hardening behavior of fly ash-based geopolymer composites [17,29,30]. Indeed a brittle geopolymer matrix could have a ductile behavior with an appropriate fiber reinforcement [29]. Pseudo strain hardening (PSH) behavior (i.e., strain hardening behavior of brittle matrix attained by fiber reinforcement) was reported with deformation over 4% during tensile test [29,30]. Moreover, multiple micro cracking with average crack width 45 μm was observed [29]. Similar results have been obtained with slag-based geopolymers [31,32] reinforced with polyethylene fibers. This combination resulted in PSH with strain up to 7.50% exhibiting multiple micro cracks with crack spacing less than 2.25 μm. The compressive strength was in range 36.3–54.8 MPa.

Given the lack of studies on the mechanical behavior of fiber reinforced AALS and encouraging findings with similar materials, the experimental investigation detailed in this paper aims to give a contribution to the improvement of the mechanical properties (e.g., post-peak behavior, tensile strength, and ductility) of AALS using fibrous reinforcement. The AALS matrix, optimized in previous study [7], was reinforced with polypropylene (PP) fibers. Usually hydrophobic fibers give weak bond with cementitious matrix [33]. Consequently, the surface modified PP fibers as reinforcement of HPFRCC were adopted in this investigation for their peculiar hydrophilic feature. This is the first attempt to attain PSH behavior on PP fiber reinforced AALS. In this paper, the enhancement of the PP-fiber reinforced AALS mechanical performance is experimentally demonstrated for different properties, namely: flexural, compressive, fracture toughness, and tensile behavior.

2. Materials and experimental methods

The mechanical performance of the reinforced AALS was investigated considering multifilament-PP fiber (PP-MF, Fig. 1a) and split-film-PP fiber (PP-SF, Fig. 1b). The properties of the components and the manufacturing features are detailed in this section.

2.1. Materials and manufacturing procedure

2.1.1. Fibers

In terms of HPFRCC and ECC, PP fiber is usually used along with polyvinyl alcohol (PVA) fiber in order to take advanced of different mechanical and chemical properties [34,35]. The disadvantages of using PVA fibers in cementitious materials are high bonding to the cementitious matrix leading to the fiber breakage during the pull-out process, and comparatively high cost [34]. PP fiber, on the other hand, has lower Young's modulus but higher elongation at break than PVA fiber. Therefore, using PP fiber, as in the present investigation, can bring to more mechanical compatibility and cost efficiency. In Ref. [36], PP fibers were successfully used to have strain hardening ordinary Portland cement based materials.

Both PP-MF and PP-SF fiber were kindly provided by Baumhueter Extrusion GmbH (Germany). Their properties are collected in Table 1. The adopted PP fibers were coated with a hydrophilic layer in order to improve the bonding strength between fibers and cementitious matrix. According to [17,37,38], a volume fraction of fiber of 2% was chosen to have PSH behavior of ECC. Therefore, in this study, a 2% content of PP fiber in both MF and SF shape was employed to observe the effects of each reinforcement on the mechanical behavior of AALS. Split-film fibers are obtained by cutting fibrillated tapes (i.e., split yarns), and have the same features as conventional MF fiber productions (e.g., spun fibers) such as tensile strength, elongation at break, and work potential [39,40].

2.1.2. Alkali-activated ladle slag

The LS was supplied by SSAB, Finland. The as-received slag was collected prior to being exposed to actual weather conditions (i.e., air humidity and rain). The fraction used in experiments was a fine fraction below 8 mm and had a d_{50} value of approximately 57 μm. The chemical composition of the LS, as shown in Table 2, was analyzed by X-ray fluorescence (PANalytical Omnian Axiosmax) at 4 kV. The free CaO measured by the method described in the standard EN 450-1 was zero. Additionally, particle size plays an important role in the activated reaction. Consequently, the received LS was milled with a ball mill (TPR-D-950-V-FU-EH by Germatec, Germany) to reach a d_{50} value of less than 10 μm. Every two kilograms of LS was ground for 2 h in a 10-L chamber with the filling ratio of 60%. The particle size distribution

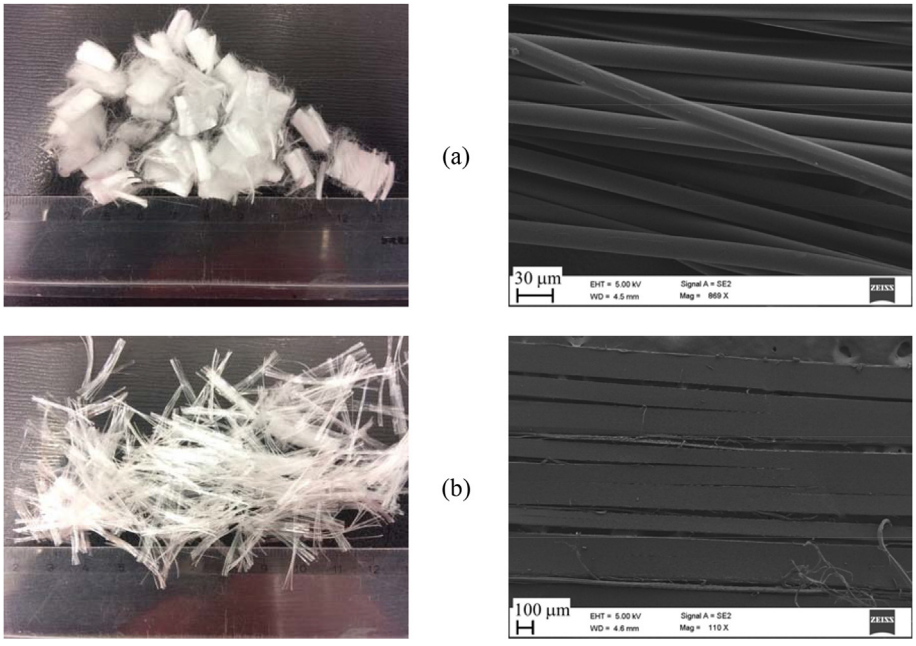

Fig. 1. Images of (a) PP-MF (b) PP-SF captured by digital camera (left) and SEM (right).

Table 1
Properties of PP fiber.

ID	Type	Young's modulus (GPa)	Elongation at break (%)	Tensile strength (MPa)	Length (mm)	Diameter*, thickness** (μm)	Density (g/cm^3)
PP-MF	Multi-fiber	1	100–200	> 220	12	20*	0.91
PP-SF	Split-film fiber	4	11	> 340	20	38**	0.91

Table 2
Chemical composition (wt %) of LS measured by XRF.

Oxide	CaO	SiO_2	Al_2O_3	Fe_2O_3	MgO	SO_3	Others
LS	46.3	8.6	28.3	5.0	7.4	0.5	3.9

after that was analyzed by a laser diffraction technique (Beckman Coulter 13 320) using the Fraunhofer model [41]. The d_{50} of milled LS was 9.16 μm.

The alkali activator was a combined solution of Na_2SiO_3 (K47791221644, Merck KGaA) and KOH (B1148333535, Merck KGaA). The Na_2SiO_3 solution containing 66.5% of water has 3.5 in modulus M_s (SiO_2/Na_2O). KOH (M = 56.11 g/mol) was in pellets. According to the optimization studied in Ref. [7], Na_2SiO_3 and KOH were mixed with a weight ratio of 0.67 and 0.03, respectively, to LS. Moreover, in order to gain a 30-min initial working time, borax (11648, Riedel-de Haen) was ground by Retsch RS200 for 30 s and then used as a retarder in mortar; the borax content was calculated based on the percentage of geopolymer solid (see the details in Ref. [42]). The details of mixture are in Table 3.

Sand fineness has been found advantageous in fiber reinforced cementitious composites [37,38]. Consequently, for the present materials, standard sand (DIN EN 196-1) was milled for 1 h with filling ratio of 60% to achieve fine sand (FS) (d_{50}: 1450 μm).

2.1.3. Fiber reinforced mortar sample preparation

The preparation of mortar specimens had the following steps. Na_2SiO_3 solution and KOH pellets were weighted and dissolved by using magnetic stirring with speed 210 rpm for 20 min. The solution was cooled down at room temperature for at least 5 h before using. Borax was gradually poured into the cooled solution and stirred for 10 min at 210 rpm. LS, FS, and PP fibers were weighted, dried and mixed in a 5-L Kenwood mixer at low (100 rpm) and high (200 rpm) speed for 1 min at each level. The alkali activating solution was added gradually to the dry mixture. The mortar was mixed at low speed for 1 min and at high speed for 2 min. During the process, the mortar was checked periodically to have a proper fibers dispersion in the mortar. Mortar samples were casted into molds and accurately vibrated for 3 min with frequency of 1 Hz. Samples were cured in plastic bags at room temperature for 24 h before demolding. Bagged-curing at room temperature was applied for samples after demolding.

2.2. Experimental devices and procedures

The effects of PP fiber reinforcements on AALS were measured and observed considering some main mechanical properties as obtained by flexural, compressive, tensile and fracture toughness tests. These can provide a clear understanding on the performance of PP fibers reinforced AALS.

Table 3
Mix proportions of the AALS reinforced with PP fiber (*Borax content was calculated as percentage of geopolymer solid, see details in Refs. [38,42]).

Sample ID	Slag	Sand	Na_2SiO_3	KOH	Borax*	PP fiber	Fiber volume fraction
2PP-MF/ 2PP-SF	1	0.5	0.67	0.03	0.2%	PP-MF/ SF	2%

Tensile and fracture toughness tests were assisted by an optical system LaVision StrainMaster [43] acquiring images at a frequency of 1 Hz. Post processing of images by the Digital Image Correlation (DIC) techniques [44] allows measurement of the full-filed displacement and calculation of the strain distribution over the surface previously speckled with black and white acrylic paints. A LED illumination was used to highlight the speckle pattern region. The lens was a Ricoh Imager M-Lite 2M; the aperture and shutter speed of camera was set to f/4.0 and 800μs, respectively.

Two software were used and compared for DIC analyses, namely DaVis 8.2 [43] and VIC-2D [45]. Some of the adopted parameters for correlation were: subset size 37, step size 3, filter size 15. Those were selected considering that lower values of subset and step sizes did not generate considerable variation of the calculated strain filed.

2.2.1. Bending

The three-point bending test, according to the standard [46] was conducted by a device Zwick (load cell of 100 kN), after 7 and 28 days of curing in a plastic bag at room temperature, six specimens for each of the considered materials. The purpose was to determine the flexural properties of mixtures compared to the reference unreinforced material. The prismatic shape of the specimen was scaled as in Ref. [7] to total length of 80 mm, width 20 mm, and height 20 mm. The supports span was 40 mm. In Ref. [47], the authors concluded that the size effect on the flexural strength of HPFRCC is negligible when conducting 3-point and 4-point bending tests. The 3-point scheme was considered in the present investigation with a displacement speed of 0.4 mm/min.

The flexural strength and stiffness were estimated, respectively, by:

$$\sigma_b = \frac{3Fl}{2bh^2} \quad E_b = \frac{ml^3}{4bh^3} \tag{1}$$

Where: σ_b is flexural strength; E_b is initial bending elastic modulus. F is maximum load; l is supports distance; b is width and h is height of the specimen. m is the initial slop of force-displacement curve.

2.2.2. Unconfined compressive strength

The compressive strength was measured according to the standard [46]. After bending failure, halves of the prismatic bending specimens were loaded on a surface of 20 mm × 20 mm, after 7 and 28 days of curing. Twelve specimens were tested for each combination and each curing time with the same Zwick device (load cell of 100 kN). The displacement speed was set to 1 mm/min.

2.2.3. Fracture toughness

The fracture toughness was investigated by the three-points bending loading of notched specimens according to RILEM 1985 TC50-FMC [48]. Fig. 2 shows the scheme of the three points bending test and the geometry of the notched specimen.

The dimensions of the specimen were: total length 160 mm, supports span 120 mm, height 40 mm, and width 40 mm. The notch depth was 20 mm, and the width was 1 mm. The three-point bending test was conducted, after seven days curing in plastic bags at room temperature, by the same loading device for the bending tests. The displacement-loading rate was 0.4 mm/min. Fracture energy was estimated by:

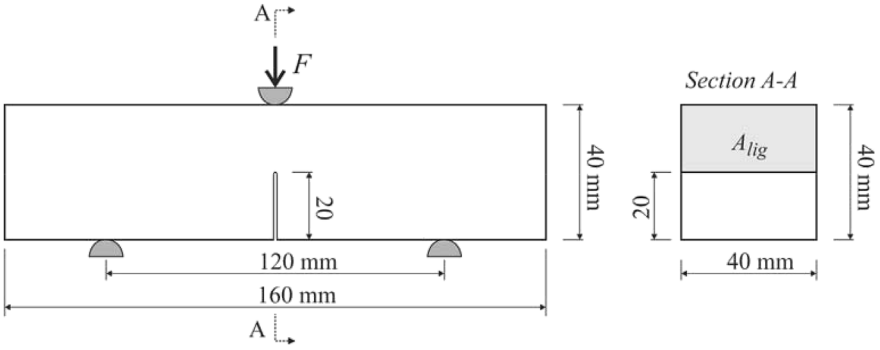

Fig. 2. Scheme of the fracture toughness test (mode I) for notched specimen.

$$G_F = \frac{\int_0^{\delta_0} p(\delta)\, d\delta \; + \; mg\delta_0}{A_{lig}} = \frac{W_0 + mg\delta_0}{A_{lig}} \tag{2}$$

Where: W_0 is fracture work; m is the weight of specimen between two supports; g is the acceleration of gravity (i.e., 9.8 m/s^2); δ_0 is the span-deflection of specimen at failure; A_{lig} is ligament area (see Fig. 2).

Fracture toughness and Young's modulus were also calculated by effective crack model suggested by Karihaloo and Nallathambi (1990) [49]. In Ref. [17], the same model to compute the fracture toughness and elastic modulus was adopted for an ECC. The Young's modulus and fracture toughness were estimated by Eqns. (3) and (4), respectively:

$$E_m = \frac{0.416P_i}{\delta_i}\left[\frac{l^3\left(1+\frac{5\omega l}{8P_i}\right)}{4bd^3\left(1-\frac{a}{d}\right)^3} + \frac{1.17l}{1.68bd\left(1-\frac{a}{d}\right)}\right] \tag{3}$$

Where P_i is arbitrary load level in the initial slop of the load-deflection curve; δ_i is its corresponding deflection; l, b, and d are span, width, and height of specimen, respectively; a is initial notch depth; and ω is self-weight of the specimen per unit length.

$$K_{Ic}^e = \sigma_n \sqrt{a_e}\, Y(\alpha) \tag{4}$$

Where $\sigma_n = 6M/(bd^2)$, in which $M = [P_{max} + (\omega l/2)](l/4)$; a_e is effective notch depth which can be derived from Eqn. (3) by substituting P_i and δ_i by max load $P_{\max}$ and the mid-span deflection at peak load δ_p; and $Y(\alpha)$ is the correction factor calculated by:

$$Y(\alpha) = \frac{1.99 - \alpha(1-\alpha)(2.15 - 3.93\alpha + 2.70\alpha^2)}{(1+2\alpha)(1-\alpha)^{1.5}} \tag{5}$$

with $\alpha = a_e/d$.

The aim of DIC measurements was the observation of the initiation and development of the cracks pattern, during complete fracture toughness test, by a contactless method. Cracks were detected in the higher strain concentration zones. The measurements were also considered to estimate and compare the crack mouth opening displacement (CMOD).

2.2.4. Uniaxial tension

Uniaxial tension tests were performed on dog-bone specimens with dimensions recommended by Japan Society of Civil Engineers for HPFRCC [50]. The adopted main geometrical features are: width 30 mm, thickness 13 mm, total length 330 mm and free length of constant width 80 mm. The specimen geometry was successfully used in Refs. [29,32]. The tensile tests of specimens cured in plastic bags for seven days were performed with a machine MTS 810 (maximum load capacity set to 10 kN) setting a loading rate of 0.5 mm/min.

3. Results and discussion

The experimental results provided an overview on the modification of some mechanical properties, compared to the reference plain material, of the AALS mortars reinforced by PP-MF and PP-SF. Beside the compression and bending mechanical features, the influence of the reinforcement was assessed observing by scanning electron microscope (SEM) the failure surface of bent specimens and the global compressive failure mode. The fracture toughness tests provided, also, an understanding on the crack initiation and development by the DIC technique. Finally, the tensile behavior clarified the response of materials including post-peak behavior and cracks propagation under uniaxial tensile load observed by DIC. Experimental results revealed that the PP fibers offered relevant improvements in the mechanical performance of AALS mortars under different loading conditions. Additionally, the PP-SF had better effects on cementitious matrix than the PP-MF.

3.1. Bending

For the comparison of pre-peak properties, the average flexural strength and stiffness are collected in Fig. 3. Both parameters were calculated by Eqn. (1) for specimens after 7 and 28 days of curing.

The flexural strength of both reinforced materials were significantly enhanced in comparison to the plain material (see Fig. 3a). The increase was ranged approximately 300% and 280% at both curing periods for 2PP-MF and 2PP-SF, respectively. This is in contrast to the negative influence of PP fiber, as reported in Refs. [33,51], on the long-term flexural strength and the negligible effect on the early ages of fly ash and slag based geopolymer. The reason was attributed to the hydrophobic nature of PP fiber which weakened the interfacial bonding strength between fibers and cementitious matrix; the fibers therefore easily detach from the matrix [52]. The better performance of PP-MF and PP-SF in this investigation is, hence, mainly connected to the hydrophilic nature of the adopted fibers, which allows for a proper load transfer between matrix and fibers. Additionally, the two reinforcements provide similar improvement of flexural strength after both 7 and 28 days of curing.

The elastic modus of materials was not affected by adding fibrous reinforcements. After 7 days curing, flexural stiffness of both reinforced materials was lower than that of the reference (see Fig. 3b). The drop was by 18% and 13% with PP-MF and PP-SF, respectively. Similar results were reported in Ref. [51]. Additionally, the 2PP-SF generated a slightly stiffer behavior than that of 2PP-MF after both 7 days and 28 days. This can be related to the difference in Young's modulus between PP-SF (i.e., 4 GPa) and PP-MF (i.e., 1 GPa) (see Table 1). After 28 days curing, all materials indicated similar stiffness due to probably an improved interfacial bonding between reinforcements and AALS matrix by time.

The PP fibers changed the post peak behavior of AALS composites completely which highlighted one of the main effects (i.e., the bridging of cracks) of the two reinforcements. Typical stress vs. mid-span deflection curves for the reinforced and plain materials are compared in Fig. 4. The plain material showed a typical brittle failure after reaching

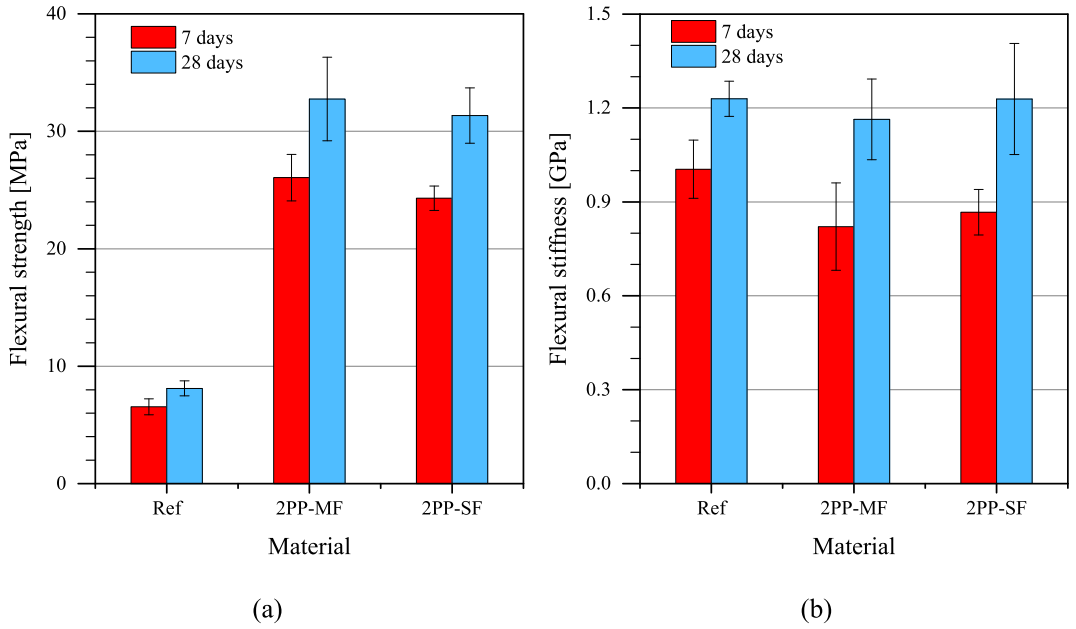

Fig. 3. Flexural (a) strength and (b) stiffness of materials after 7 and 28 days of curing.

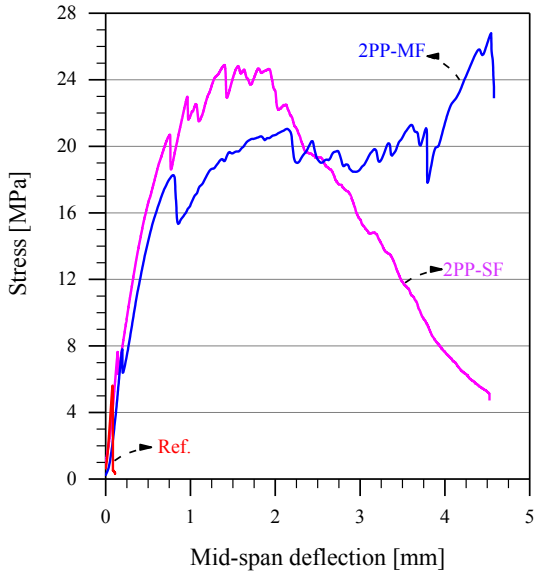

Fig. 4. Flexural tests: representative load vs. mid-span deflection curves after 7 days of curing.

peak load while the 2PP-MF and 2PP-SF exhibited pseudo strain hardening (PSH) behavior with a huge increase of load after the level at the onset of initial crack. Interestingly, the initial crack load level of reinforced mortars (approximately 7.9 MPa) were higher than that of the reference one (approximately 5.6 MPa); this is probably related to the good bond of fibers and cementitious matrix leading, as mentioned, to a proper load transfer and load carrying of the fibers at the early stage. Under fiber bridging effect, the fibers delayed the crack propagation and the sudden failure of brittle AALS. In Ref. [53], PSH behavior was observed when using 2% v/v PP fiber in concrete, while in Ref. [54], a PP fiber volume fraction of 0.5% indicated only strain softening behavior. Furthermore, the bridging effect was distinct between PP-MF and PP-SF, as indicated in Fig. 4. After initial crack, the 2PP-SF had a PSH branch up to the peak load and then the material exhibited softening behavior with loading level slowly decreasing while increasing the deflection. The 2PP-MF, on the other hand, had a PSH branch up to about 2 mm of deflection, then a plateau with almost stable load level and finally the fibers provided a further contribution to increase the load carrying capacity of the material.

The effect of fibers resulted in a higher global bending deformation with relevant increasing of the failure mid-span deflection of the specimens. The observation of the fracture surface by SEM captured at the same two magnifications can explain locally the influence of the reinforcements on the failure mechanics. The fracture surface of plain material highlights typical brittle failure with crack propagation along interfacial transition zone between AALS and FS (see Fig. 5a). The reinforced specimens show less smooth fracture surfaces due to the cracks deviation around the fibers (see Fig. 5b and c). Fig. 5b and c indicate the fiber bridging effect of PP-MF and PP-SF leading to wider cracks at failure than the reference material. Furthermore, the dispersed fibers had some residual mortar still in adhesion (Fig. 5c). This shows a good bonding between fibers and AALS and an efficient load-transfer mechanism from matrix to reinforcements. Consequently, higher energy spent on de-bonding and cracks development with fiber bridging. This explains at the macroscale the different post-peak behavior between the plain and fibrous reinforced materials (see Fig. 4). The 2PP-MF and 2PP-SF absorbed significantly larger amount of energy for propagating cracks resulting in a 'ductile' behavior of the reinforced materials.

3.2. Compression

The compressive strength of all materials illustrates the distinct effect between the PP-MF and PP-SF on the composites. The strength was measured after 7 and 28 days of curing. In comparison to the reference material (see Fig. 6), the 2PP-MF fibers had no beneficial effect on the compressive strength. On one hand, the strength of reference and 2PP-MF reinforced materials reached almost the ultimate value after 7 days. On the other hand, the 2PP-SF after 28 days enhanced the compressive strength by approximately 24% compared to the plain material and by 46% compared to its strength after 7 days of curing. In contrast, a reduction was reported in Ref. [51] when 1% PP fiber was used in slag based alkaline cement mortars tested after 28 curing days. Generally, HPFRCC exhibits higher compressive strength than unreinforced material, however conflicting results are also reported in literature (see e.g., [55]).

The AALS is a high-early-strength cementitious material that meets requirements in Ref. [56]. This depends on the fast rate of hydration

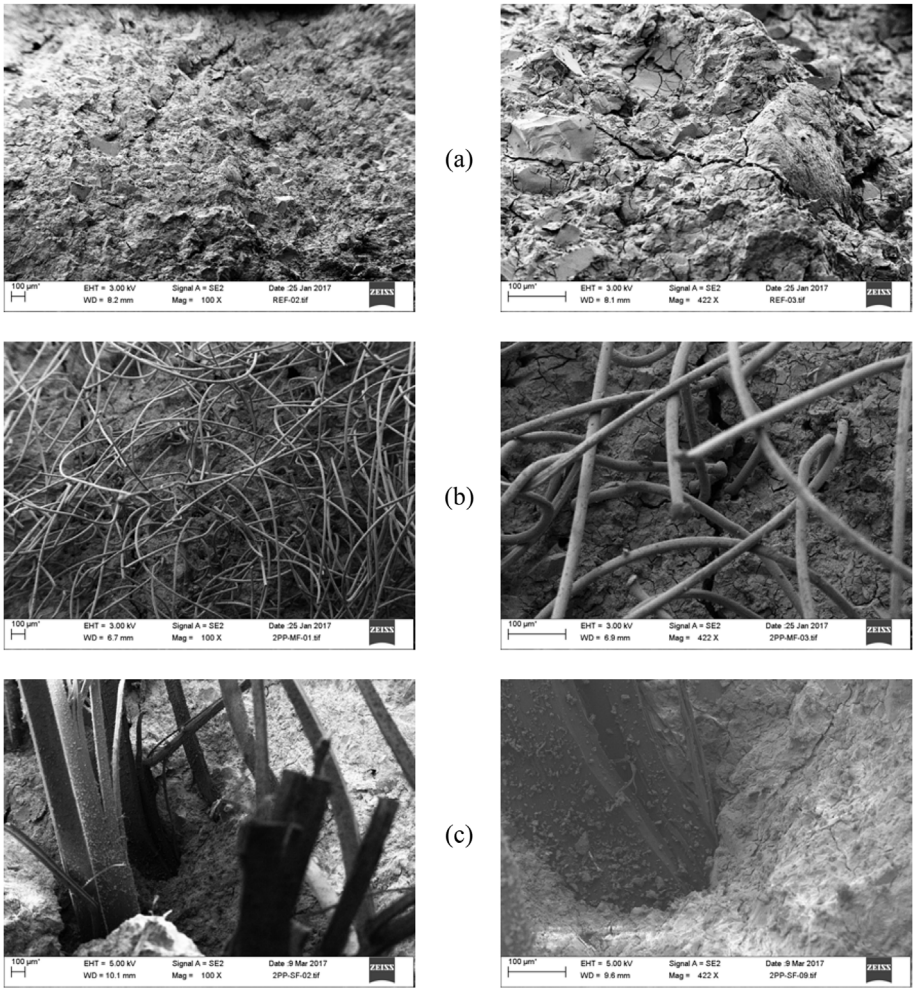

Fig. 5. Flexural tests after 7 days of curing: SEM images of the fracture surface (a) Reference; (b) 2PP-MF; (c) 2PP-SF.

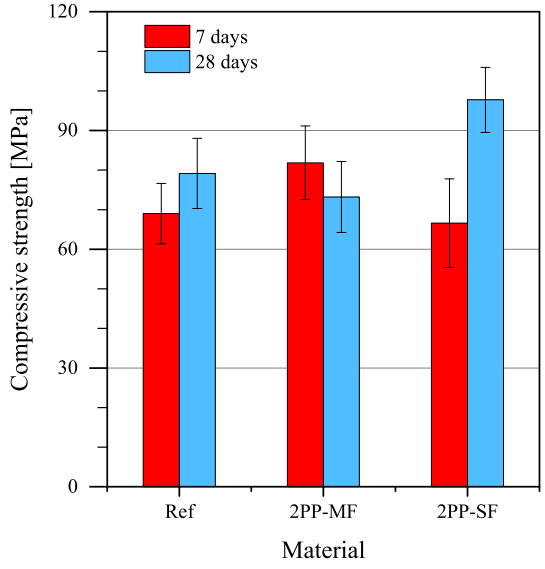

Fig. 6. Compressive strength of materials after 7 and 28 days of curing.

reactions at elevated pHs of slags, as reported in Ref. [57]. In comparison to Portland cement, where the main bonding phase is C-S-H, semicrystalline C-(N)-A-S-H in alkali-activated slag presents a high proportion of aluminum in the tetrahedral bridges and interlayer calcium substitution by sodium leading to a lower Ca/Si ratio than that of Portland cement [58,59]. Semicrystalline C-(N)-A-S-H is the main strength-giving phase in AALS; also, this structure leads to a better compressive strength of AALS.

Regarding failure mode under compression, both 2PP-MF and 2PP-SF showed branching of several cracks resulting in a 'ductile' behavior, while the reference had a typical failure of brittle material with the evolution of one main crack through the specimen (see Fig. 7). In reinforced materials, fibers delayed the evolution of the cracks resisting to micro-crack extension. As a consequence, the diffuse pattern of micro cracks is bridged by the fibers and therefore the driving force for the cracks is curtailed [60].

3.3. Fracture toughness

Fracture toughness quantifies the capacity of a material to resist crack initiation and propagation, and is therefore an important property to measure. Fracture toughness as well as uniaxial tensile tests were supposed on specimens cured for 7 days, due to the high early strength (Fig. 6), and the results are assumed applicable also for longer curing periods.

The plain material showed typical brittle behavior, while the reinforced AALS composites had much better load carrying capacity at post peak branch. The response of materials under fracture tests is initially represented in Fig. 8a. The first visible effect of both PP-MF and PP-SF reinforcements is the increase of the load level at onset of crack opening, namely approximately 370 N, 530 N and 550 N for reference, 2PP-MF and 2PP-SF, respectively. The reference material indicated a

Fig. 7. Failure mode under compression after 28 days of curing: (a) Reference; (b) 2PP-MF; (c) 2PP-SF.

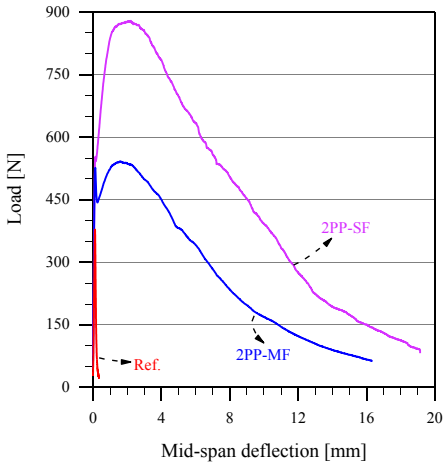

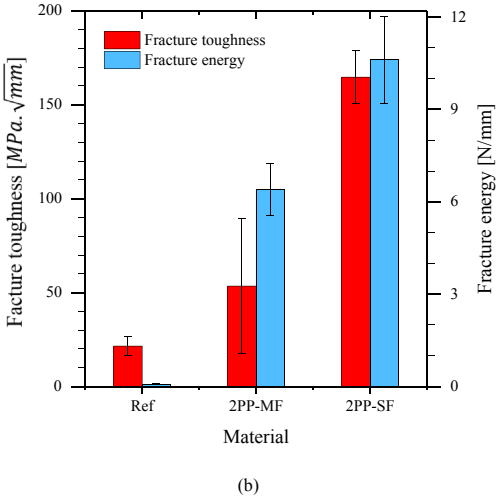

Fig. 8. Fracture toughness tests: a) representative load vs. mid-span deflection curves b) fracture energy GF and fracture toughness K_{Ic} at failure.

typical brittle behavior in which the load dropped dramatically after reaching the peak. Compared to the reference material, the 2PP-MF and 2PP-SF performed differently with much better load carrying capacity after initial crack appeared. Similar results were reported in the literature with cotton fiber [61], macro steel and PP fiber [62] reinforced fly ash based geopolymer. The extension of the post-peak branch up to failure had different shape for the two PP reinforcements. The mid-span deflection at the complete unloading of reinforced materials was roughly 30–40 times higher than that of the plain material. Furthermore, the post peak maximum load of the PP-SF was considerable higher than the PP-MF showing a better bridging effect for mode I crack opening (see Fig. 8a).

Fracture toughness tests highlight an important improvement offered by the PP-MF and PP-SF to the AALS. The above qualitative comparison (underlined mainly for the peak, post-peak maximum load and mid-span deflection of the materials) was quantified considering the fracture energy and the fracture toughness calculated by Eqns. (2) and (4), respectively. The comparison in Fig. 8b shows the average fracture energy of mortar with 2PP-MF and 2PP-SF almost 90 and 150 times larger than the unreinforced material, respectively. Moreover, the 2PP-SF attained average fracture energy roughly 65% larger than that of the 2PP-MF. In comparison, an increase by almost 40 times compared to the plain material in terms of fracture energy was reported in Ref. [63] for cement mortar reinforced with carbon fiber reinforced polymer waste. Regarding the fracture toughness, fibrous reinforcements offered a noticeable improvement by 2.5 and 7.6 times for 2PP-MF and 2PP-SF, respectively, compared to the reference material. In Ref. [61], a maximum increase of 3 times was achieved by using 8.3 wt% of cotton fibers in geopolymer.

The observed improvement of the fibrous composites was confirmed by measuring the CMOD by the DIC contactless technique. Some representative load-CMOD curves are compared in Fig. 9. The addition of PP fibers completely modified the post-peak behavior, as observed above (see Figs. 8a and 9), with large CMOD and high load levels. The curves in Fig. 9 have a similar shape to that obtained in Refs. [63,64] using fibers reinforced cement mortars. They have three turning points, which are distinguishable in the curves of reinforced materials, including the peak load (L1), the minimum post-cracking load (L2) at the end of the descending initial softening behavior and the maximum post-cracking remaining load (L3) of the reloading process. The L2 is supposed when the fibers start absorbing the energy released by the mortar in the fracture processes by fiber bridging and change the loading tendency. The L3 is considered as the maximum capacity of fibers to absorb the fracture energy [65]. The 2PP-SF had very small difference of L1 and L2 both in terms of load and CMOD levels. This means that

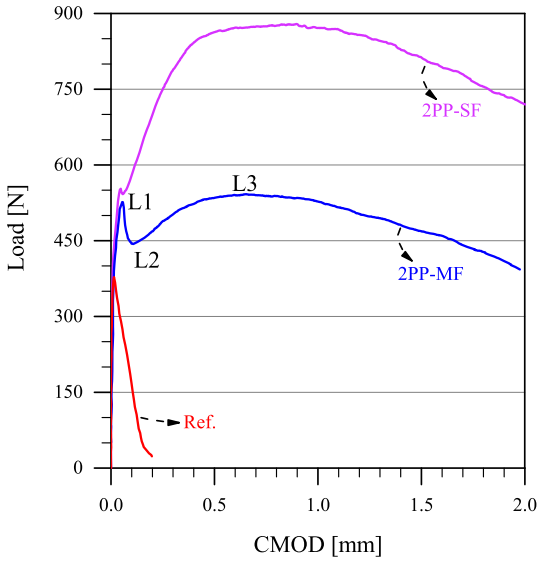

Fig. 9. Fracture toughness tests: representative load vs. CMOD measured by DIC.

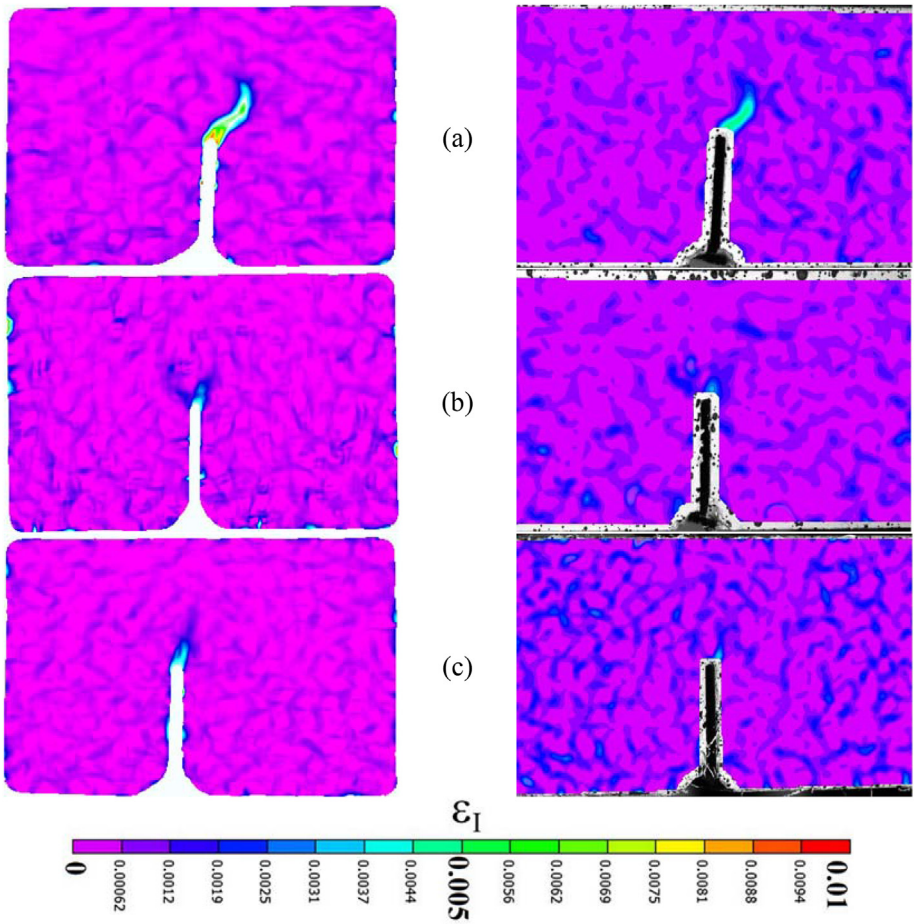

Fig. 10. Fracture toughness tests: comparison of maximum principal strain (ε_I) maps as calculated by StrainMaster (left) and VIC-2D (right) at peak load of the reference material (378 N). (a) Reference, (b) 2PP-MF and (c) 2PP-SF specimen.

the PP-SF started fiber bridging and energy absorption immediately after the onset and propagation of initial crack. In contrast, the 2PP-MF had higher decrease of load with slightly increase of CMOD probably related to the deformation of the fibers within the crack.

The PP fibers controlled crack propagation and led to a higher load level under fracture mode I tests. Strain maps calculated by StrainMaster and VIC-2D for some fracture toughness tests are compared in Fig. 10. The images were captured at the peak load of the specimen for reference material (almost 378 N). Both software were able to detect the crack as its appearance. At the peak load of the plain material, the crack had a fast propagation with a length covering almost one third of the ligament height. The very beginning of the crack onset was also detected for the 2PP-MF and 2PP-SF materials at the same load level (see Fig. 10b and c). However its propagation was immediately controlled and confined by the bridging of the fibers leading to an increase of the load up to a higher peak (Figs. 8a and 9) and a delay of the crack propagation (Fig. 9). The bridging effect of PP fibers is confirmed comparing the crack length developed in the fracture process zone as measured for the specimens at the load level in Fig. 10. The crack length of the plain material was roughly 8 mm, while the crack of PP-MF and PP-SF was around 1.2 and 1.5 mm, respectively.

Overall, the PP-SF had better effects on the AALS than the PP-MF in term of energy absorbing, fiber bridging and fiber pulling-out (Figs. 8–10). This is also reflected on the fracture surface (Fig. 11). The images show the distribution of fibers in AALS matrix and the fiber pulling-out behavior under fracture toughness tests. The fracture surface of reference sample is very sharp and flat while the PP fibers in reinforced mortars made the fracture surface rougher with an almost uniform distribution of pull-out and broken fibers.

3.4. Uniaxial tension

PSH behavior was observed on PP fiber reinforced AALS under uniaxial tensile tests, as exhibited in Fig. 12. The strain was measured by StrainMaster with a virtual strain gage (gage length 70 mm). The reference materials indicated a typical stress-strain curve for brittle materials; the stress dropped sharply after hitting the peak load (approximately 1.9 MPa) with a small strain. In contrast, the reinforced materials showed a PSH behavior after the onset of initial crack for a load level higher than 2.2 MPa. The stress-performance index (i.e., the peak of crack bridging stress to initial crack stress ratio proposed in Ref. [66]) of 2PP-MF and 2PP-SF was 1.2 and 1.3, respectively. After the first crack onset, the 2PP-MF and 2PP-SF exhibited PSH behavior under fiber bridging effect with an increase in peak load of 18% and 27%, respectively, in comparison to the initial crack load. Similar results in literature were reported on PP fibers [16,67] or hybrid PP-PVA fibers [35] reinforced Portland cement based ECC. Interestingly, the 2PP-SF absorbed more energy under uniaxial tensile load than the 2PP-MF, while the latter had a smaller softening post-peak branch with a lower strain at failure (see Fig. 12).

The good bridging effect of PP fibers helped the fibers carry tensile load at the early stage and reach to higher loading level than the plain material. The comparison of average first crack and maximum tensile stress levels in Fig. 13 shows that the plain material had the same value for the two stress levels, meaning crack appeared at the peak tensile load. While, the 2PP-MF and 2PP-SF exhibited considerable PSH behavior as demonstrated stress-performance index [18,37]. Furthermore, the first crack stress level of reinforced materials was higher than that of the plain material with an increase of approximately 93% and 62%

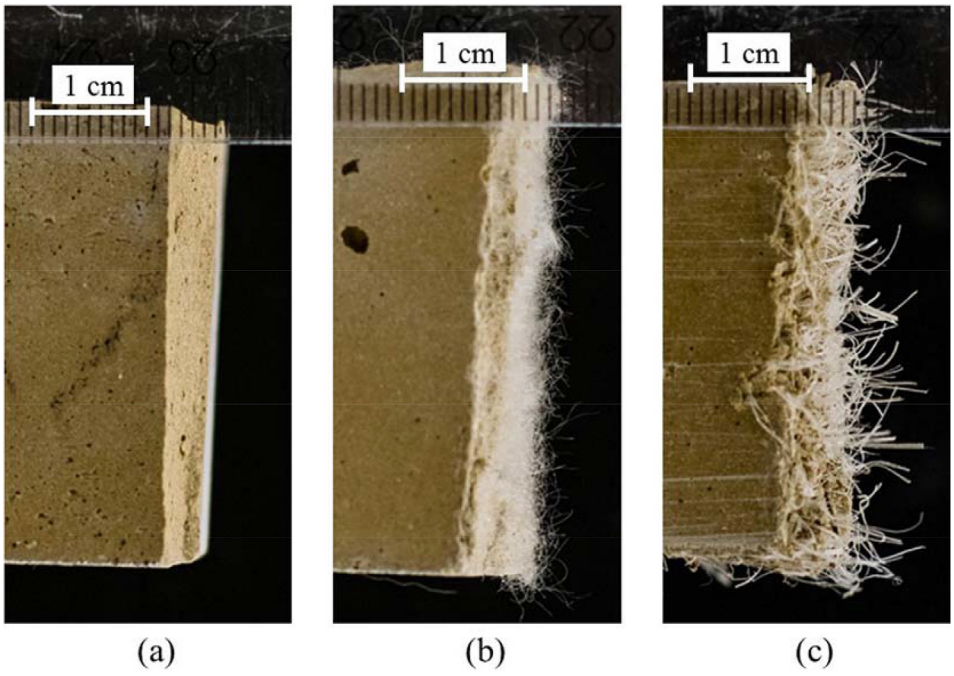

Fig. 11. Fracture toughness tests: representative fracture surface of: (a) Reference, (b) 2PP-MF and (c) 2PP-SF.

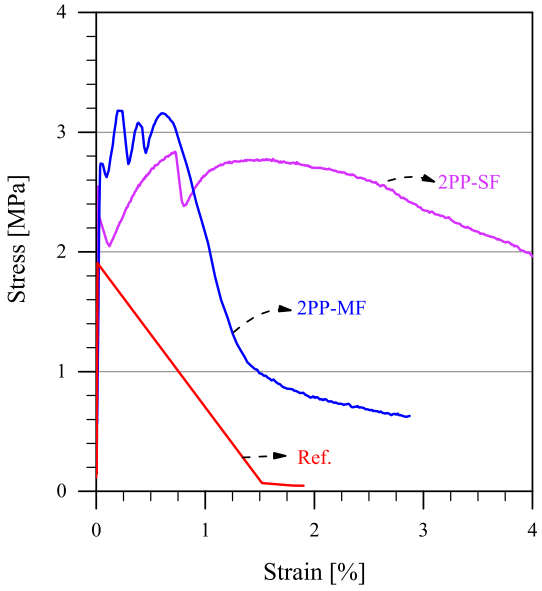

Fig. 12. Tensile test: stress-strain measured by DIC.

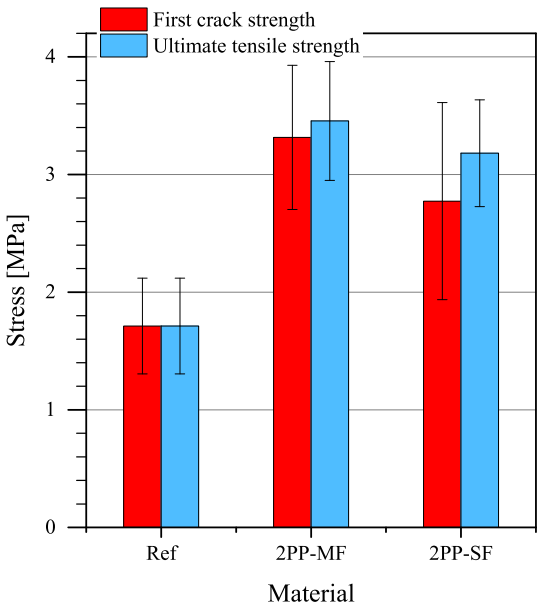

Fig. 13. Tensile test: first crack and maximum stress levels.

for 2PP-MF and 2PP-SF, respectively. In terms of ultimate tensile strength, the reinforced materials increased the stress by roughly 80% compared to the reference material. Additionally, the difference between 2PP-MF and 2PP-SF in terms of initial crack and ultimate tensile strength was not relevant.

The observation by DIC confirms the PSH behavior of reinforced materials compared to the reference. Fig. 14 indicates the cracks pattern and maximum principal strain map at the maximum load for the reference (almost 1.95 MPa) and at the load level for the development of the last crack in the 2PP-MF and 2PP-SF (approximately 3.15 and 2.75 MPa, respectively). The maps were calculated by both StrainMaster (Fig. 14 left) and VIC-2D (Fig. 14 right). The unreinforced material generated only one macro crack, while multiple cracks were recorded on the 2PP-MF and 2PP-SF specimens. The strain map of 2PP-MF illustrates more multiple cracks along DIC area of interest than that of 2PP-SF. Similar result was revealed in Ref. [29], however, with much smaller crack size (average 45 μm) observed by DIC on fly ash based geopolymer ECC. Nevertheless, Fig. 14 clearly shows that the AALS composites improved the ductility under uniaxial tension by crack transfer mechanism that generated steady state flat cracks instead a typical Griffith crack [68]. Multiple cracks observed by DIC technique proved the PSH behavior shown in Fig. 12. This improvement once again confirms the positive effect of the adopted PP fiber types on the mechanical behavior of AALS.

4. Conclusions

Alkali-activated ladle slag (AALS) can improve the mechanical performance and become ‘ductile’ with proper amount and properties

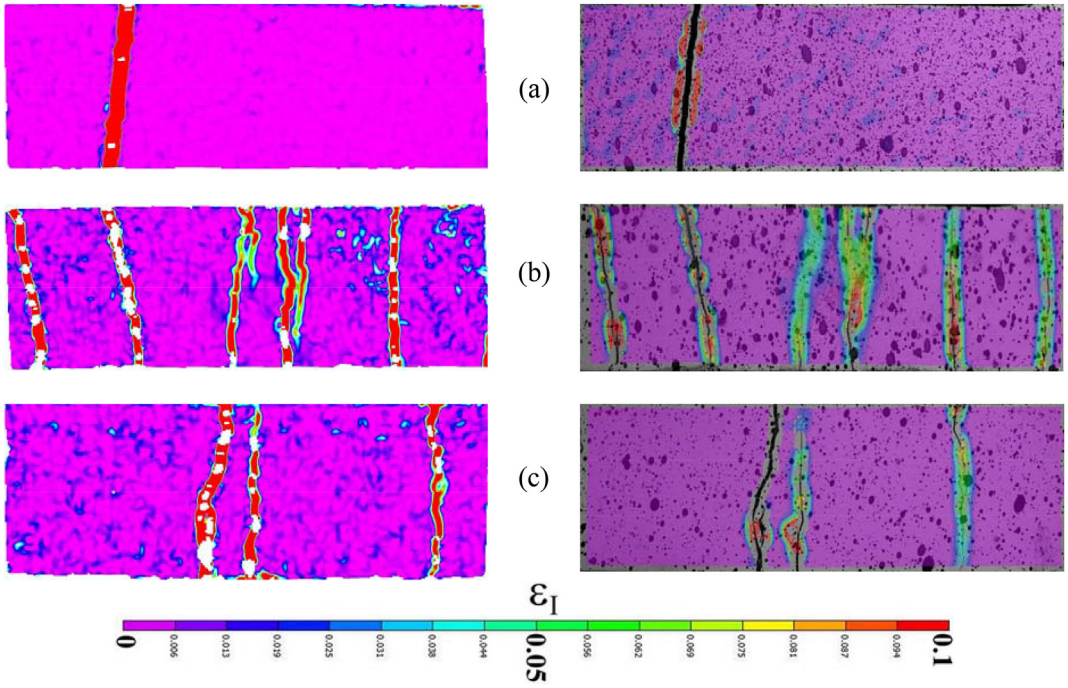

Fig. 14. Tensile tests: comparison of cracks distribution and maximum principal strain (ε_I) maps at failure (load direction is horizontal) as calculated by StrainMaster (left) and VIC-2D (right): (a) Reference, (b) 2PP-MF and (c) 2PP-SF.

of fibrous reinforcement. This is the main result of the present investigation, as similarly obtained in the literature for other alkali-activated materials (e.g., alkali activated fly ash and blast furnace slag). Under laboratory testing conditions, pseudo strain hardening (PSH) behavior was recorded with 2% PP fiber reinforced AALS, while the reference material exhibited typical brittle behavior. This results in multiple cracks pattern of the PP enhanced materials, as observed by DIC technique, under uniaxial tension.

The mechanical properties of AALS mortars reinforced by multi-filament-PP fiber (PP-MF) or split-film-PP fiber (PP-SF) reveals that the effect of hydrophilic PP fibers is evident with increment by 300%, 80%, 7.6 times, and 150 times in flexural, tensile strength, fracture toughness, and fracture energy, respectively. Furthermore, the PP-SF offers better mechanical response than the PP-MF in post peak load carrying capacity of the reinforcement during mode I fracture development and uniaxial tension.

This investigation gives a contribution to the development of high performance alkali-activated materials using fibrous reinforcements for their possible adoption in construction industry. However, further investigation need addressing: optimization of the fibers content, durability in aggressive environments, damage mechanisms, and thermal and shrinkage properties.

Acknowledgements

This work was supported by the European Regional Development Fund [grant number: A70189]. The contributions of Jyri Porter, Matias Jaskari, Antti Järvenpää and Tun Tun Nyo (University of Oulu) to mechanical tests are gratefully acknowledged. The authors appreciate support from Baumhueter Extrusion GmbH (Germany) and SSAB (Finland) for providing PP fibers and ladle slag, respectively, in this study.

References

[1] N.M. Piatak, M.B. Parsons, R.R. Seal II, Characteristics and environmental aspects of slag: A review, Environ. Geochem. Mod. Min. 57 (2015) 236–266, http://dx.doi.org/10.1016/j.apgeochem.2014.04.009.

[2] Statistics 2012, EUROSLAG, http://www.euroslag.com/products/statistics/2012/, (2012).

[3] E.K. Anastasiou, I. Papayianni, M. Papachristoforou, Behavior of self compacting concrete containing ladle furnace slag and steel fiber reinforcement, Mater. Des. 59 (2014) 454–460, http://dx.doi.org/10.1016/j.matdes.2014.03.030.

[4] J. García-Cuadrado, A. Rodríguez, I.I. Cuesta, V. Calderón, S. Gutiérrez-González, Study and analysis by means of surface response to fracture behavior in lime-cement mortars fabricated with steelmaking slags, Construct. Build. Mater. 138 (2017) 204–213, http://dx.doi.org/10.1016/j.conbuildmat.2017.01.122.

[5] B. Nematollahi, R. Ranade, J. Sanjayan, S. Ramakrishnan, Thermal and mechanical properties of sustainable lightweight strain hardening geopolymer composites, Arch. Civ. Mech. Eng. 17 (2017) 55–64, http://dx.doi.org/10.1016/j.acme.2016.08.002.

[6] B.C. McLellan, R.P. Williams, J. Lay, A. van Riessen, G.D. Corder, Costs and carbon emissions for geopolymer pastes in comparison to ordinary portland cement, J. Clean. Prod. 19 (2011) 1080–1090, http://dx.doi.org/10.1016/j.jclepro.2011.02.010.

[7] E. Adesanya, K. Ohenoja, P. Kinnunen, M. Illikainen, Alkali activation of ladle slag from steel-making process, J. Sustain. Metall. (2016) 1–11, http://dx.doi.org/10.1007/s40831-016-0089-x.

[8] A. Natali Murri, W.D.A. Rickard, M.C. Bignozzi, A. van Riessen, High temperature behaviour of ambient cured alkali-activated materials based on ladle slag, Cement Concr. Res. 43 (2013) 51–61, http://dx.doi.org/10.1016/j.cemconres.2012.09.011.

[9] M.C. Bignozzi, S. Manzi, I. Lancellotti, E. Kamseu, L. Barbieri, C. Leonelli, Mix-design and characterization of alkali activated materials based on metakaolin and ladle slag, Geopolymers New Smart Way Sustain. Dev. 73 (2013) 78–85, http://dx.doi.org/10.1016/j.clay.2012.09.015.

[10] V. Li, Engineered cementitious composite (ECC), Concr. Constr. Eng. Handb, CRC Press, 2008, https://doi.org/10.1201/9781420007657.ch24.

[11] A.E. Naaman, H.W. Reinhardt, High performance fiber reinforced cement composites HPFRCC-4: international RILEM workshop, Mater. Struct. 36 (2003) 710–712, http://dx.doi.org/10.1007/BF02479507.

[12] G. Chanvillard, S. Rigaud, Complete Characterisation of Tensile Properties of Ductal® UHPFRC According to the French Recommendations, RILEM Publications SARL, 2003, p. 14.

[13] P. Rossi, A. Arca, E. Parant, P. Fakhri, Bending and compressive behaviours of a new cement composite, Cement Concr. Res. 35 (2005) 27–33, http://dx.doi.org/10.1016/j.cemconres.2004.05.043.

[14] V.C. Li, T. Hashida, Engineering ductile fracture in brittle-matrix composites, J. Mater. Sci. Lett. 12 (1993) 898–901, http://dx.doi.org/10.1007/BF00455611.

[15] S.H. Park, D.J. Kim, G.S. Ryu, K.T. Koh, Tensile behavior of ultra high performance hybrid fiber reinforced concrete, Cement Concr. Compos. 34 (2012) 172–184, http://dx.doi.org/10.1016/j.cemconcomp.2011.09.009.

[16] S. Boughanem, D.A. Jesson, M.J. Mulheron, P.A. Smith, C. Eddie, S. Psomas, M. Rimes, Tensile characterisation of thick sections of Engineered Cement Composite (ECC) materials, J. Mater. Sci. 50 (2015) 882–897, http://dx.doi.org/10.1007/s10853-014-8649-6.

[17] B. Nematollahi, J. Sanjayan, F. Ahmed Shaikh, Tensile strain hardening behavior of PVA fiber-reinforced engineered geopolymer composite, J. Mater. Civ. Eng. 27

(2015), http://dx.doi.org/10.1061/(ASCE)MT.1943-5533.0001242 04015001.
[18] V.C. Li, H.-C. Wu, Conditions for pseudo strain-hardening in fiber reinforced brittle matrix composites, Appl. Mech. Rev. 45 (1992) 390–398, http://dx.doi.org/10.1115/1.3119767.
[19] M. Sahmaran, G. Yildirim, T.K. Erdem, Self-healing capability of cementitious composites incorporating different supplementary cementitious materials, Cement Concr. Compos. 35 (2013) 89–101, http://dx.doi.org/10.1016/j.cemconcomp.2012.08.013.
[20] B. Suryanto, J.O. Buckman, P. Thompson, M. Bolbol, W.J. McCarter, Monitoring micro-crack healing in an engineered cementitious composite using the environmental scanning electron microscope, Mater. Char. 119 (2016) 175–185, http://dx.doi.org/10.1016/j.matchar.2016.07.021.
[21] H.-J. Kong, S.G. Bike, V.C. Li, Development of a self-consolidating engineered cementitious composite employing electrosteric dispersion/stabilization, Cement Concr. Compos. 25 (2003) 301–309, http://dx.doi.org/10.1016/S0958-9465(02)00057-4.
[22] H.-J. Kong, S.G. Bike, V.C. Li, Constitutive rheological control to develop a self-consolidating engineered cementitious composite reinforced with hydrophilic poly (vinyl alcohol) fibers, Cement Concr. Compos. 25 (2003) 333–341, http://dx.doi.org/10.1016/S0958-9465(02)00056-2.
[23] S. Wang, V.C. Li, High-early-strength engineered cementitious composites, ACI Mater. J. 103 (2006) 97–105.
[24] E. Shaheen, N.G. Shrive, Cyclic loading and fracture mechanics of Ductal® concrete, Int. J. Fract. 148 (2007) 251–260, http://dx.doi.org/10.1007/s10704-008-9199-1.
[25] Q. Li, B. Huang, S. Xu, B. Zhou, R.C. Yu, Compressive fatigue damage and failure mechanism of fiber reinforced cementitious material with high ductility, Cement Concr. Res. 90 (2016) 174–183, http://dx.doi.org/10.1016/j.cemconres.2016.09.019.
[26] H.-D. Yun, K. Rokugo, Freeze-thaw influence on the flexural properties of ductile fiber-reinforced cementitious composites (DFRCCs) for durable infrastructures, Cold Reg. Sci. Technol. 78 (2012) 82–88, http://dx.doi.org/10.1016/j.coldregions.2012.02.002.
[27] Y. Zhu, Y. Yang, Y. Yao, Autogenous self-healing of engineered cementitious composites under freeze–thaw cycles, Construct. Build. Mater. 34 (2012) 522–530, http://dx.doi.org/10.1016/j.conbuildmat.2012.03.001.
[28] A.R. Sakulich, Reinforced geopolymer composites for enhanced material greenness and durability, Sustain. Cities Soc. 1 (2011) 195–210, http://dx.doi.org/10.1016/j.scs.2011.07.009.
[29] M. Ohno, V.C. Li, A feasibility study of strain hardening fiber reinforced fly ash-based geopolymer composites, Construct. Build. Mater. 57 (2014) 163–168, http://dx.doi.org/10.1016/j.conbuildmat.2014.02.005.
[30] B. Nematollahi, J. Sanjayan, F.U.A. Shaikh, Strain hardening behavior of engineered geopolymer composites: effects of the activator combination, J. Australas. Ceram. Soc. 51 (2015) 54–60.
[31] J.-I. Choi, K.-I. Song, J.-K. Song, B.Y. Lee, Composite properties of high-strength polyethylene fiber-reinforced cement and cementless composites, Compos. Struct. 138 (2016) 116–121, http://dx.doi.org/10.1016/j.compstruct.2015.11.046.
[32] J.-I. Choi, B.Y. Lee, R. Ranade, V.C. Li, Y. Lee, Ultra-high-ductile behavior of a polyethylene fiber-reinforced alkali-activated slag-based composite, Cement Concr. Compos. 70 (2016) 153–158, http://dx.doi.org/10.1016/j.cemconcomp.2016.04.002.
[33] N. Ranjbar, S. Talebian, M. Mehrali, C. Kuenzel, H.S. Cornelis Metselaar, M.Z. Jumaat, Mechanisms of interfacial bond in steel and polypropylene fiber reinforced geopolymer composites, Compos. Sci. Technol. 122 (2016) 73–81, http://dx.doi.org/10.1016/j.compscitech.2015.11.009.
[34] H. Pakravan, M. Jamshidi, M. Latifi, The effect of hybridization and geometry of polypropylene fibers on engineered cementitious composites reinforced by polyvinyl alcohol fibers, J. Compos. Mater. 50 (2015) 1007–1020, http://dx.doi.org/10.1177/0021998315586078.
[35] H.R. Pakravan, M. Jamshidi, M. Latifi, Study on fiber hybridization effect of engineered cementitious composites with low- and high-modulus polymeric fibers, Construct. Build. Mater. 112 (2016) 739–746, http://dx.doi.org/10.1016/j.conbuildmat.2016.02.112.
[36] L. Bang Yeon, L. Victor C, K. Yun Yong, Polypropylene fiber-based strain-hardening cementitious composites, Proceeding of the World Congress on Advances in Structural Engineering and Mechanics ASEM13, September 8-12, 2013, pp. 444–457 Jeju, Korea.
[37] V.C. Li, D.K. Mishra, H.-C. Wu, Matrix design for pseudo-strain-hardening fibre reinforced cementitious composites, Mater. Struct. 28 (1995) 586–595, http://dx.doi.org/10.1007/BF02473191.
[38] B. Nematollahi, J. Sanjayan, F.U.A. Shaikh, Matrix design of strain hardening fiber reinforced engineered geopolymer composite, Compos. B Eng. 89 (2016) 253–265, http://dx.doi.org/10.1016/j.compositesb.2015.11.039.
[39] A. Pellegrini, P. Olivieri, W. Schoene, M. Schweizer, Fibers, 7. Polyolefin fibers, Ullmanns Encycl. Ind. Chem. Wiley-VCH Verlag GmbH & Co. KGaA, 2000, , http://dx.doi.org/10.1002/14356007.o10_o03.
[40] H. Krässig, Film to fiber technology, J. Polym. Sci. Macromol. Rev. 12 (1977) 321–410, http://dx.doi.org/10.1002/pol.1977.230120105.
[41] ISO 13320:2009, Particle Size Analysis – Laser Diffraction Methods, International Organization for Standardization, (2009).
[42] S.E.W. Djwantoro Hardjito Dody, M.J. Sumajouw, B. Vijay, Rangan, on the development of fly ash-based geopolymer concrete, Mater. J. 101 (2004), http://dx.doi.org/10.14359/13485.
[43] LaVision StrainMaster, (2016) http://www.lavision.de/en/products/strainmaster/index.php , Accessed date: 27 January 2017.
[44] M.A. Michael, A.J.-J. Orteu, H.W. Schreier, Digital image correlation (DIC), in: H. Schreier, J.-J. Orteu, M.A. Sutton (Eds.), Image Correl. Shape Motion Deform. Meas. Basic ConceptsTheory Appl. Springer US, Boston, MA, 2009, pp. 1–37, , http://dx.doi.org/10.1007/978-0-387-78747-3_5.
[45] Correlated Solutions – VIC-2D™, (2016) http://correlatedsolutions.com/vic-2d/ , Accessed date: 15 March 2017.
[46] ISO 679:2009, Cement – Test Methods – Determination of Strength, International Organization for Standardization, (2009).
[47] Kay Wille, Gustavo J. Parra-Montesinos, Effect of beam size, casting method, and support conditions on flexural behavior of ultra-high-performance fiber-reinforced concrete, Mater. J. 109 (2012), http://dx.doi.org/10.14359/51683829.
[48] Determination of the fracture energy of mortar and concrete by means of three-point bend tests on notched beams, Mater. Struct. 18 (1985) 287–290, http://dx.doi.org/10.1007/BF02472918.
[49] B.L. Karihaloo, P. Nallathambi, Effective crack model for the determination of fracture toughness (KIce) of concrete, Eng. Fract. Mech. 35 (1990) 637–645, http://dx.doi.org/10.1016/0013-7944(90)90146-8.
[50] Recommendations for design and construction of high performance fiber reinforced cement composites with multiple fine cracks, Concr. Eng. Ser. 82, JSCE, Japan, 2008.
[51] F. Puertas, T. Amat, A. Fernández-Jiménez, T. Vázquez, Mechanical and durable behaviour of alkaline cement mortars reinforced with polypropylene fibres, Cement Concr. Res. 33 (2003) 2031–2036, http://dx.doi.org/10.1016/S0008-8846(03)00222-9.
[52] B. Felekoğlu, K. Tosun, B. Baradan, Effects of fibre type and matrix structure on the mechanical performance of self-compacting micro-concrete composites, Cement Concr. Res. 39 (2009) 1023–1032, http://dx.doi.org/10.1016/j.cemconres.2009.07.007.
[53] V. Corinaldesi, A. Nardinocchi, Influence of type of fibers on the properties of high performance cement-based composites, Construct. Build. Mater. 107 (2016) 321–331, http://dx.doi.org/10.1016/j.conbuildmat.2016.01.024.
[54] H.A. Toutanji, Properties of polypropylene fiber reinforced silica fume expansive-cement concrete, Construct. Build. Mater. 13 (1999) 171–177, http://dx.doi.org/10.1016/S0950-0618(99)00027-6.
[55] V. Afroughsabet, L. Biolzi, T. Ozbakkaloglu, High-performance fiber-reinforced concrete: a review, J. Mater. Sci. 51 (2016) 6517–6551, http://dx.doi.org/10.1007/s10853-016-9917-4.
[56] ASTM C150/C150M-16e1, Standard Specification for Portland Cement, ASTM International, West Conshohocken, PA, 2016www.astm.org.
[57] Y. Ding, J.-G. Dai, C.-J. Shi, Mechanical properties of alkali-activated concrete: a state-of-the-art review, Construct. Build. Mater. 127 (2016) 68–79, http://dx.doi.org/10.1016/j.conbuildmat.2016.09.121.
[58] I.G. Richardson, J.G. Cabrera, The nature of C-S-H in model slag-cements, Cem. Concr. Compos 22 (2000) 259–266, http://dx.doi.org/10.1016/S0958-9465(00)00022-6.
[59] V.O. Özçelik, C.E. White, Nanoscale charge-balancing mechanism in alkali-substituted calcium–silicate–hydrate gels, J. Phys. Chem. Lett. 7 (2016) 5266–5272, http://dx.doi.org/10.1021/acs.jpclett.6b02233.
[60] V.C. Li, A simplified micromechanical model of compressive strength of fiber-reinforced cementitious composites, Spec, Issue Micromechanics Fail. Cem. Compos 14 (1992) 131–141, http://dx.doi.org/10.1016/0958-9465(92)90006-H.
[61] T. Alomayri, F.U.A. Shaikh, I.M. Low, Synthesis and mechanical properties of cotton fabric reinforced geopolymer composites, Compos. B Eng. 60 (2014) 36–42, http://dx.doi.org/10.1016/j.compositesb.2013.12.036.
[62] A. Bhutta, P.H.R. Borges, C. Zanotti, M. Farooq, N. Banthia, Flexural behavior of geopolymer composites reinforced with steel and polypropylene macro fibers, Cement Concr. Compos. 80 (2017) 31–40, http://dx.doi.org/10.1016/j.cemconcomp.2016.11.014.
[63] H. Nguyen, V. Carvelli, T. Fujii, K. Okubo, Cement mortar reinforced with reclaimed carbon fibres, CFRP waste or prepreg carbon waste, Construct. Build. Mater. 126 (2016) 321–331, http://dx.doi.org/10.1016/j.conbuildmat.2016.09.044.
[64] M.G. Alberti, A. Enfedaque, J.C. Gálvez, Fracture mechanics of polyolefin fibre reinforced concrete: study of the influence of the concrete properties, casting procedures, the fibre length and specimen size, Eng. Fract. Mech. 154 (2016) 225–244, http://dx.doi.org/10.1016/j.engfracmech.2015.12.032.
[65] M.G. Alberti, A. Enfedaque, J.C. Gálvez, On the mechanical properties and fracture behavior of polyolefin fiber-reinforced self-compacting concrete, Construct. Build. Mater. 55 (2014) 274–288, http://dx.doi.org/10.1016/j.conbuildmat.2014.01.024.
[66] T. Kanda, V.C. Li, Practical design criteria for saturated pseudo strain hardening behavior in ECC, J. Adv. Concr. Technol. 4 (2006) 59–72, http://dx.doi.org/10.3151/jact.4.59.
[67] R. Zhang, K. Matsumoto, T. Hirata, Y. Ishizeki, J. Niwa, Application of PP-ECC in beam–column joint connections of rigid-framed railway bridges to reduce transverse reinforcements, Eng. Struct. 86 (2015) 146–156, http://dx.doi.org/10.1016/j.engstruct.2015.01.005.
[68] V.C. Li, On engineered cementitious composites (ECC), J. Adv. Concr. Technol. 1 (2003) 215–230, http://dx.doi.org/10.3151/jact.1.215.